



# Molecular Gas Properties in Young Stellar Clusters with a Suppressed Star Cluster Wind

Sergiy Silich<sup>1</sup> , Jean Turner<sup>2</sup> , Jonathan Mackey<sup>3</sup> , and Sergio Martínez-González<sup>1</sup> <sup>1</sup>Instituto Nacional de Astrofísica Óptica y Electrónica, AP 51, 72000, Puebla, México; [silich@inaoep.mx](mailto:silich@inaoep.mx)<sup>2</sup>UCLA Department of Physics and Astronomy, Los Angeles, CA, 90095-1547, USA<sup>3</sup>Dublin Institute for Advanced Studies, Astronomy & Astrophysics Section, DIAS Dunsink Observatory, Dublin, D15 XR2R, Ireland

Received 2022 November 28; revised 2023 January 23; accepted 2023 January 27; published 2023 February 15

## Abstract

In compact and dense star-forming clouds a global star cluster wind could be suppressed. In this case stellar feedback is unable to expel the leftover gas from the cluster. Young massive stars remain embedded in a dense residual gas and stir it by moving in the gravitational well of the system. Here we present a self-consistent model for the molecular gas distribution in such young, enshrouded stellar clusters. It is assumed that the cloud collapse terminates and the star formation ceases when a balance between the turbulent pressure and gravity and between the turbulent energy dissipation and regeneration rates is established. These conditions result in an equation that determines the residual gas density distribution that, in turn, allows one to determine the other characteristics of the leftover gas and the star formation efficiency. It is shown that our model predictions are in good agreement with several observationally determined properties of cloud D1 in the nearby dwarf spheroidal galaxy NGC 5253 and its embedded cluster.

*Unified Astronomy Thesaurus concepts:* [Star clusters \(1567\)](#)

## 1. Introduction

Star formation has been a fundamental problem in astrophysics for many years. There is general agreement that star formation requires dense molecular gas and occurs in giant molecular clouds. It was shown a long time ago that the interstellar gas depletion time in our Galaxy is much longer than the freefall time of molecular clouds (e.g., Williams & McKee 1997), which raised the problem of molecular cloud stability and apparently low average star formation efficiency (SFE) in our and other galaxies. Different solutions to these problems have been proposed and include strong magnetic fields (e.g., Shu et al. 1987), photoionization of intracloud gas (McKee 1989; Franco et al. 1994), and different modifications to the feedback scenario—the injection of energy and momentum into the residual molecular gas by low-mass (Norman & Silk 1980; McKee 1989) or high-mass (Matzner 2002) stars (see the review by Padoan et al. 2014).

In contrast, to form a bound stellar cluster a large (>30%) SFE is required (Baumgardt & Kroupa 2007; Baumgardt et al. 2008). This raises the question how to prevent or at least retard the leftover gas expulsion and the molecular cloud disruption at early stages of massive star cluster formation (e.g., Wirth et al. 2022 claimed that it took 3.5–4.0 Myr to stop star formation in Galactic globular clusters).

Supersonic velocity dispersions have been detected in objects of different scales from the cores of molecular clouds and compact, young stars still enshrouded by molecular gas stellar clusters, to giant H II regions and H II galaxies. This led Terlevich & Melnick (1981), Solomon et al. (1987), and Melnick et al. (1987) to suggest that supersonic turbulence is a characteristic of the gas virial equilibrium and that dynamic feedback from newborn stars prevents the parental cloud from further collapsing.

Tenorio-Tagle et al. (1993) associated supersonic velocities with a collection of bow shocks around pre-main-sequence stars moving in the gravitational well of the cluster and suggested that these bow shocks stir and maintain supersonic turbulence until massive stars and supernovae expel the remaining gas from the cluster. However, supersonic turbulence decays very rapidly (Stone et al. 1998; Mac Low 1999), which requires sources more powerful than low-mass stars to maintain supersonic turbulence in star-forming clouds (e.g., Murray et al. 2010). Different aspects of supersonic turbulence in molecular clouds were reviewed by, among others, Scalo (1987), Vazquez-Semadeni et al. (2000), Elmegreen & Scalo (2004), Mac Low & Klessen (2004), McKee & Ostriker (2007), and Padoan et al. (2014). Bow shocks, their turbulent mixing layers, and wakes were also discussed by many authors (see Arthur & Hoare 2006; Wareing et al. 2007; Binette et al. 2009; Mackey et al. 2013, 2015; Henney & Arthur 2019, and references therein).

The role of massive stars in turbulent energy regeneration was discussed by Matzner (2002) who considered H II regions as the major mechanism for turbulent energy regeneration, but did not discuss the effects of the intracluster gas distribution.

Marks & Kroupa (2012) found that the initial star cluster half-mass radius weakly depends on stellar mass (see their Equation (7)) and even for  $10^5$ – $10^6 M_{\odot}$  clusters, it hardly exceeds 1 pc. In such compact and massive star-forming regions wind-driven bubbles around individual massive stars stall before merging with their neighbors (see Silich & Tenorio-Tagle 2017, 2018) and ionizing photons are effectively absorbed by dust grains which reemit them in the infrared (IR) wave band. Upon such conditions massive stars are not able to photoionize the bulk of leftover gas, form a global star cluster wind, or expel the residual gas from the star-forming region. The negative stellar feedback is then suppressed. Instead, ultracompact H II regions (UCH II) embedded in the residual molecular gas form (Silich et al. 2020). However, Silich & Tenorio-Tagle (2017, 2018) considered only mechanical equilibrium in star-forming clouds with an arbitrary

selected SFE and did not account for rapid turbulent energy dissipation.

Here, following Norman & Silk (1980), McKee (1989), and Matzner (2002) we assume that the pre-stellar cloud collapse is followed by vigorous star formation that terminates when a balance between the turbulent pressure and gravity and the turbulent energy dissipation and regeneration rates is established. In contrast with other authors (e.g., Padoan 1995; Krumholz & McKee 2005; Krumholz et al. 2006; Padoan & Nordlund 2011), we do not consider how star formation proceeds in the collapsing cloud, but assume that it results in a stellar cluster with a certain mass and a known stellar density distribution, and that further star formation is altered by stellar feedback. It is also postulated that the cluster is sufficiently compact and dense to prevent leftover gas expulsion, the post-star-forming system is dynamically stable, and that stellar feedback compensates the turbulent energy dissipation continuously. Our aim is to find out how the leftover molecular gas is distributed and obtain its other characteristics under such conditions. We show that the equilibrium conditions together with the only one free parameter that characterizes the degree to which the feedback energy could be conserved, as well as fixing the residual gas density, velocity dispersion, and temperature distributions, allows one to estimate the SFE if the stellar mass distribution is known.

The paper is organized as follows. In Section 2 we select a model for the stellar mass distribution. In Section 3 the conditions for thermal and mechanical equilibrium are formulated and the equation that determines the residual gas density distribution is derived. We demonstrate then that the velocity dispersion and the SFE in the post-star-forming cloud follow directly from the equilibrium conditions and the gas density distribution. In Section 3.3 we discuss the major sources for the molecular gas heating and cooling and show how to determine the molecular gas temperature. In Section 4 we confront our model with the well studied molecular cloud D1 in the nearby dwarf spheroidal galaxy NGC 5253 and show that the model predictions are in agreement with several observational characteristics of this cloud and its embedded cluster. Finally, in Section 5 we summarize our findings and the major model restrictions.

## 2. Stellar Mass Distribution

Hereafter it is assumed that star formation in the parental molecular cloud results in a dense compact cluster with a total stellar mass  $M_{\text{SC}}$  and a Gaussian stellar density distribution:

$$\rho_*(r) = \frac{M_{\text{SC}}}{(2\pi)^{3/2}b^3} \exp\left[-\frac{1}{2}\left(\frac{r}{b}\right)^2\right], \quad (1)$$

$$n_*(r) = \frac{N_*}{(2\pi)^{3/2}b^3} \exp\left[-\frac{1}{2}\left(\frac{r}{b}\right)^2\right], \quad (2)$$

where  $\rho_*$  is the stellar mass density,  $N_*$  and  $n_*$  are the total number and the number density of the turbulence-driven stars, respectively, and  $b$  is the star cluster core radius.

The stellar mass  $M_*(r)$  enclosed within a sphere of radius  $r$  then is:

$$M_*(r) = M_{\text{SC}} \left[ \text{erf}\left(\frac{r}{2^{1/2}b}\right) - \left(\frac{2}{\pi}\right)^{1/2} \frac{r}{b} \exp\left[-\frac{1}{2}\left(\frac{r}{b}\right)^2\right] \right], \quad (3)$$

where  $\text{erf}(r)$  is the error function.

## 3. Equilibrium Conditions

### 3.1. Turbulent Energy Dissipation and Regeneration Rates

Following Stone et al. (1998), Mac Low (1999), and Basu & Murali (2001) we assume that the rate of turbulent energy dissipation in the residual gas is:

$$Q_{\text{dis}}(r) = \frac{\eta_d \rho_g \sigma^3}{\lambda}, \quad (4)$$

where  $\rho_g$  and  $\sigma$  are the residual gas density and 1D velocity dispersion, respectively, and  $\lambda$  is the turbulence-driving scale. The dimensionless factor  $\eta_d \sim 1$  over a range of driving lengths (see Basu & Murali 2001, and references therein). We assume that  $\eta_d = 1$  in all our simulations.

In spite of many discussions (e.g., Basu & Murali 2001; Quillen et al. 2005; Swift & Welch 2008; Brunt et al. 2009), the nature and the value of the driving length remain uncertain. Here we postulate that turbulence in a newborn cluster is supported by massive stars that randomly move in the gravitational well of the cluster. It is likely that in such a case the driving length  $\lambda$  is determined by the separations between neighboring massive stars. The plausible assumption then is that half of the driving wavelength is equal to the mean distance between two neighboring massive stars and thus  $\lambda = 4X$ , where  $X$ , the half-distance between neighboring massive stars, is (see Silich et al. 2020):

$$X(r) = b \left[ (9\pi/2)^{1/2} \exp\left[\frac{1}{2}\left(\frac{r}{b}\right)^2\right] \right]^{1/3} N_*^{-1/3}. \quad (5)$$

Note that in this case the driving length is not constant, as adopted in most models, but depends on the distance from the star cluster center (multi-scale energy injection was discussed by Scalo 1987). This assumption results in the turbulent energy dissipation rate:

$$Q_{\text{dis}}(r) = \frac{\eta_d \rho_g \sigma^3 N_*^{1/3}}{4(9\pi/2)^{1/6} b \exp\left[\frac{1}{6}\left(\frac{r}{b}\right)^2\right]}. \quad (6)$$

We assume that the lost turbulent energy is regenerated in the turbulent mixing layers and turbulent wakes formed around most massive stars that move in the gravitational well of the cluster. We further follow arguments presented in Norman & Silk (1980), McKee (1989), and Matzner (2002) and assume that recently formed stars support turbulence in the residual gas at the rate:

$$Q_*(r) = P\sigma(r)n_*(r)/2, \quad (7)$$

where  $P$  is the average rate of momentum input to the intracloud medium per massive star, which includes momentum input via stellar winds, radiation  $L_*/c$ , and is due to the photoheated H II regions expansion. The precise value of the

momentum continuously returned to the intracloud medium by a typical massive star is uncertain. Here we normalize it to the stellar radiative momentum input rate (see Henney & Arthur 2019):

$$P = \eta_* L_*/c, \quad (8)$$

where  $L_* = L_{\text{bol}}/N_*$  is the average turbulence-driving star luminosity,  $L_{\text{bol}}$  is the star cluster bolometric luminosity, and  $c$  is the speed of light. The  $\eta_*$  factor is considered as a free parameter in the model. The value of this parameter is determined by the degree to which the feedback energy could be conserved. It depends on the physical conditions in the star-forming cloud, and in general must be determined by numerical simulations. McKee (1999) suggested that  $\eta_* \approx 1.6$ , to account for energy stored in magnetic fields, while the numerical simulations by Mackey et al. (2013), which focused on the dynamics of H II regions around moving O stars, showed that the momentum input rate could exceed that provided by radiation pressure by up to 10 times. It is interesting to note that active galactic nucleus outflows also often have momentum well in excess (up to 30 times) of the central black hole integrated momentum  $L_{\text{BH}}\tau_{\text{in}}/c$ , where  $\tau_{\text{in}}$  is the characteristic timescale of radiative feedback (see Faucher-Giguère & Quataert 2012, and references therein). We adopt  $\eta_*$  in the range  $1 < \eta_* < 10$ .

In dense, compact clusters the characteristic sizes of individual wind-driven bubbles are much smaller than the cluster core radius  $b$  (Silich & Tenorio-Tagle 2017, 2018). Therefore we assume that the energy dissipation and regeneration rates are balanced locally throughout the cluster:  $Q_{\text{dis}}(r) = Q_*(r)$ . This leads to the relation:

$$\rho_g \sigma^2 = \frac{\eta_*}{\eta_d} \left( \frac{3}{4\pi^4} \right)^{1/3} \frac{L_{\text{bol}}}{cb^2 N_*^{1/3}} \exp \left[ -\frac{1}{3} \left( \frac{r}{b} \right)^2 \right]. \quad (9)$$

### 3.2. Mechanical Equilibrium

Mechanical equilibrium in a post-star-forming cloud requires the gravitational pull of the cluster to be in balance with the turbulent pressure (e.g., Calura et al. 2015):

$$\frac{dP_{\text{turb}}}{dr} = -\frac{G\rho_g(M_g(r) + M_*(r))}{r^2}, \quad (10)$$

where  $G$  is the gravitational constant,  $M_g(r)$  and  $M_*(r)$  are the gas and the stellar mass enclosed within a sphere of radius  $r$ , respectively, and  $P_{\text{turb}}(r) = \rho_g \sigma^2$  is the residual gas turbulent pressure.

### 3.3. Equilibrium Gas Distribution

Equation (9) allows one to calculate the turbulent pressure derivative  $dP_{\text{turb}}/dr = d(\rho_g \sigma^2)/dr$ . Combining this derivative with Equation (10), one can obtain an equation that determines the residual gas density distribution in a stationary post-star-forming cloud upon the assumption that the turbulent energy

dissipation is continuously compensated by stellar feedback:

$$\begin{aligned} \rho_g(r) &= \frac{\eta_*}{\eta_d} \left( \frac{2}{9\pi} \right)^{1/3} \frac{L_{\text{bol}}}{\pi c G b N_*^{1/3} [M_*(r) + M_g(r)]} \left( \frac{r}{b} \right)^3 \\ &\quad \times \exp \left[ -\frac{1}{3} \left( \frac{r}{b} \right)^2 \right] \\ &\approx 10^{-14} \frac{\eta_*}{\eta_d} \frac{L_{42}}{N_*^{1/3} b_1 [M_{*,s}(r) + M_{g,s}(r)]} \left( \frac{r}{b} \right)^3 \\ &\quad \times \exp \left[ -\frac{1}{3} \left( \frac{r}{b} \right)^2 \right] \text{ g cm}^{-3}, \end{aligned} \quad (11)$$

where  $L_{42} = L_{\text{bol}}/10^{42} \text{ erg s}^{-1}$ ,  $b_1$  is the core radius in parsec units,  $M_{*,s}(r)$  is the stellar mass, and  $M_{g,s}(r)$  is the gas mass, both in solar units. The residual gas mass in Equation (11) is:

$$M_g(r) = 4\pi \int_0^r x^2 \rho_g(x) dx. \quad (12)$$

We solve Equation (11) by iterations by making use Equation (12). At the first step it is assumed that the gas density is equal to zero in the whole star cluster volume. This implies that in Equation (11)  $M_g(r) = 0$ , but allows one to calculate a new, nonzero gas density distribution  $\rho_i(r)$  as the stellar density and stellar mass are not equal to zero. A new gas density distribution is used then to integrate Equation (12) numerically and obtain a new, nonzero gas mass distribution  $M_{g,i}(r)$ . This  $M_{g,i}(r)$  is used in Equation (11) to improve the gas density distribution. The iteration process continues until the difference between the subsequent values of the integrated gas mass becomes small enough:  $|(M_{g,i} - M_{g,i-1})|/(M_{g,i} + M_{g,i-1}) < \epsilon$ . We usually stop iterating when  $\epsilon$  drops below  $10^{-5}$ . After the residual gas distribution is calculated, one can easily obtain the other characteristics of the star-forming region. The velocity dispersion is calculated by means of Equations (9) and (11):

$$\begin{aligned} \sigma(r) &= \left[ \frac{3G(M_*(r) + M_g(r))}{2b} \right]^{1/2} \left( \frac{b}{r} \right)^{3/2} \\ &\approx 8 \times 10^{-2} \left[ \frac{M_{*,s}(r) + M_{g,s}(r)}{b_1} \right]^{1/2} \left( \frac{b}{r} \right)^{3/2} \text{ km s}^{-1}. \end{aligned} \quad (13)$$

The SFE is:

$$\text{SFE} = M_{\text{SC}}/[M_{\text{SC}} + M_g(R)], \quad (14)$$

where  $R$  is the adopted radius of the cluster. The total turbulent energy dissipation rate in the residual gas is:

$$L_{\text{gas}}(R) = 4\pi \int_0^R Q_{\text{dis}}(x) x^2 dx. \quad (15)$$

The stellar bolometric and the wind mechanical luminosities do not increase linearly with stellar mass. We estimate that only 15%–20% of massive stars contribute about 90% to the star cluster energy budget, and adopt for the number of the turbulence-driven stars:

$$N_* \approx 0.15 \times N_{\text{massive}}(M_{\text{SC}}/10^6 M_{\odot}), \quad (16)$$

where  $N_{\text{massive}}$  is the number of massive ( $M > 8 M_{\odot}$ ) stars in a  $10^6 M_{\odot}$  cluster. In clusters with a canonical Kroupa initial mass

function (IMF)  $N_{\text{massive}} \approx 1.1 \times 10^4$  (e.g., Calura et al. 2015), while in the case of a Salpeter IMF with lower and upper cutoff masses of  $3 M_{\odot}$  and  $120 M_{\odot}$ , respectively,  $N_{\text{massive}} \approx 3.1 \times 10^4$ .

### 3.4. Thermal Balance and the Molecular Gas Temperature

The thermal balance in a post-star-forming cloud is determined by the turbulent, cosmic ray (CR), and X-ray gas heating and the molecular gas cooling rates (e.g., Maloney et al. 1996; Basu & Murali 2001; Shang et al. 2002; Pan & Padoan 2009; Papadopoulos 2010):

$$Q_{\text{dis}} + Q_{\text{CR}} + Q_{\text{XR}} - Q_{\text{cool}} - Q_{\text{gd}} = 0. \quad (17)$$

In Equation (17)  $Q_{\text{dis}}$  is the turbulent energy dissipation rate (see Equation (4)),  $Q_{\text{CR}}$  and  $Q_{\text{XR}}$  are the CR and the X-ray heating rates, respectively, and  $Q_{\text{cool}}$  is the molecular gas cooling rate.  $Q_{\text{gd}}$  is the energy exchange between the gas and dust grains (see Goldsmith 2001; Pan & Padoan 2009; Papadopoulos 2010):

$$Q_{\text{gd}} = 7 \times 10^{-34} n^2 T_g^{1/2} (T_g - T_d) \text{ erg cm}^{-3} \text{ s}^{-1}, \quad (18)$$

where  $n = \rho_g / \mu_{\text{mol}}$  is the molecular gas number density,  $\mu_{\text{mol}}$  is the mean mass per particle in the molecular gas, and  $T_g$  and  $T_d$  are the molecular gas and the dust grain temperatures, respectively. We adopt  $\mu_{\text{mol}} = 2.33 m_{\text{H}}$ , where  $m_{\text{H}}$  is the hydrogen atom mass. In a UV-shielded dense environment the CR heating rate is determined by the CR ionization rate per  $\text{H}_2$  molecule (Papadopoulos 2010):

$$Q_{\text{CR}} = 1.5 \times 10^{-24} \xi_{\text{CR},17} n_4 \text{ erg cm}^{-3} \text{ s}^{-1}, \quad (19)$$

where  $\xi_{\text{CR},17}$  is the CR ionization rate in units of  $10^{-17} \text{ s}^{-1}$  and  $n_4$  is the molecular gas number density in units of  $10^4 \text{ cm}^{-3}$ . The reference value for  $\xi_{\text{CR}}$  is  $5 \times 10^{-17} \text{ s}^{-1}$ —the average CR ionization rate in our Galaxy. In compact starbursts it may be up to  $10^3$  times larger (Papadopoulos 2010).

The residual molecular gas in dense UV-shielded parcels of a star-forming cloud may be also exposed to and heated by soft and hard X-ray emission caused by magnetic line reconnection in young stellar objects, X-ray binaries, or shock-heated stellar winds (e.g., Maloney et al. 1996; Feigelson & Montmerle 1999; Shang et al. 2002; Meijerink & Spaans 2005, and references therein). For example, Tsujimoto et al. (2006) reported the detection of hard X-ray emission from the two UCH II regions in W49A, one of the most active star-forming regions in our Galaxy. The X-ray heating rate is given by (Panoglou et al. 2012; Mackey et al. 2019):

$$Q_{\text{XR}} = \eta_{\text{X}} n H_{\text{X}}, \quad (20)$$

where  $\eta_{\text{X}}$  is the heating efficiency (see Dalgarno et al. 1999),  $H_{\text{X}}$  is the X-ray energy absorption rate per particle (Maloney et al. 1996; Panoglou et al. 2012):

$$H_{\text{X}} = \int_{E_{\text{min}}}^{E_{\text{max}}} \sigma_{\text{X}}(E) F(E) dE, \quad (21)$$

where  $F(E)$  is the X-ray flux and  $\sigma_{\text{X}}(E)$  is the photoelectric cross section per H nucleus.

One can obtain the molecular gas temperature from the energy balance equation (Equation (17)) by making use a reasonable approximation for the molecular gas cooling rate

$Q_{\text{cool}} = Q_{\text{cool}}(n, T, du/dr)$ , where  $du/dr$  is the velocity gradient.

## 4. NGC 5253 Cloud D1 and its Embedded Cluster

In this section we confront our model with the NGC 5253 D1 molecular cloud and its young, compact cluster. For the star cluster mass, core radius, and metallicity we adopt  $M_{\text{SC}} = 1.625 \times 10^5 M_{\odot}$ ,  $b = 0.8 \text{ pc}$ , and  $Z = 0.2 Z_{\odot}$ , respectively (see Turner et al. 2017; Silich et al. 2020). We also adopt a canonical Kroupa IMF with lower and upper cutoffs of  $M_{\text{low}} = 0.1 M_{\odot}$  and  $M_{\text{up}} = 120 M_{\odot}$ , respectively. In this case  $N_{\star} \approx 270$ . We then make use the Starburst99 synthetic model to obtain the embedded cluster bolometric luminosity ( $L_{\text{bol}} = 3.9 \times 10^{42} \text{ erg s}^{-1}$  at an age of 1 Myr) and calculate the residual gas density distribution. The velocity dispersion is then obtained from Equation (13). The stellar mass and the model-predicted gas density distributions are presented by dotted, solid, and dashed lines in Figure 1 panel (a), while the velocity dispersion is shown in panel (b) of this figure. The dotted line in panel (a) displays the stellar density distribution derived from the Gaussian fit to the radio and IR integrated intensity maps (see Turner et al. 2000, 2015, 2017; Gorjian et al. 2001), while the solid and dashed lines present the model-predicted molecular gas distribution for  $\eta_{\star} = 1$  and  $\eta_{\star} = 5$ , respectively. The model predicts different stellar and gas density distributions with stellar mass being more concentrated toward the parental cloud center. This is consistent with the different core radii based on Gaussian fits relative to the integrated IR/radio intensity maps.

The corresponding 1D velocity dispersion is shown on panel (b). Note that the  $\eta_{\star}$  value does not affect the velocity dispersion significantly as  $\sigma \sim 1/\sqrt{\rho} \sim 1/\sqrt{\eta_{\star}}$  (see Equation (13)). For distant star-forming regions like the NGC 5253 D1 cloud, where the available spatial resolution does not allow one to study the velocity dispersion profile, one can make use of the model-predicted velocity dispersion and gas density distributions to calculate the mass-weighted velocity dispersion and compare it with the observed value:

$$\sigma_w = \frac{4\pi}{M_g(R)} \int_0^R \rho_g(x) \sigma(x) x^2 dx. \quad (22)$$

In the case of the D1 cloud the mass-weighted velocity dispersion is  $\sigma_w \approx 9.3 \text{ km s}^{-1}$  and  $\sigma_w \approx 10.4 \text{ km s}^{-1}$  in models with  $\eta_{\star} = 1$  and  $\eta_{\star} = 5$ , respectively, which is in good agreement with the observed CO linewidth ( $\sigma \approx 9.2 \text{ km s}^{-1}$ ; Turner et al. 2015, 2017). The molecular gas mass within a 7.5 pc radius in these two cases is  $M_g \approx 2.4 \times 10^4 M_{\odot}$  and  $M_g \approx 9.5 \times 10^4 M_{\odot}$ , respectively, which are consistent with the observed CO emission.

In the model-predicted density range thermal coupling between the dust grains and the molecular gas is weak (Pan & Padoan 2009; see also Appendix E in Whitworth 2016). This implies that the molecular gas temperature could be evaluated from its own energy balance and one can neglect the  $Q_{\text{gd}}$  term in Equations (17) and (24). The turbulent heating rate is about  $1.4 \times 10^{37} \text{ erg s}^{-1}$  in the simulations with  $\eta_{\star} = 1$  and  $7.5 \times 10^{37} \text{ erg s}^{-1}$  when  $\eta_{\star} = 5$ . In both cases the integrated turbulent heating exceeds the T Tauri integrated X-ray luminosity significantly:  $L_{\text{XR,TT}} = N_{\text{PMS}} \times L_{\text{XTT}} \approx 1.2 \times 10^{35} \text{ erg s}^{-1}$ , where  $N_{\text{PMS}} \approx 1.5 \times 10^6 (M_{\text{SC}}/10^6 M_{\odot})$  is the number of low-mass ( $M < 3 M_{\odot}$ ) pre-main sequence stars and

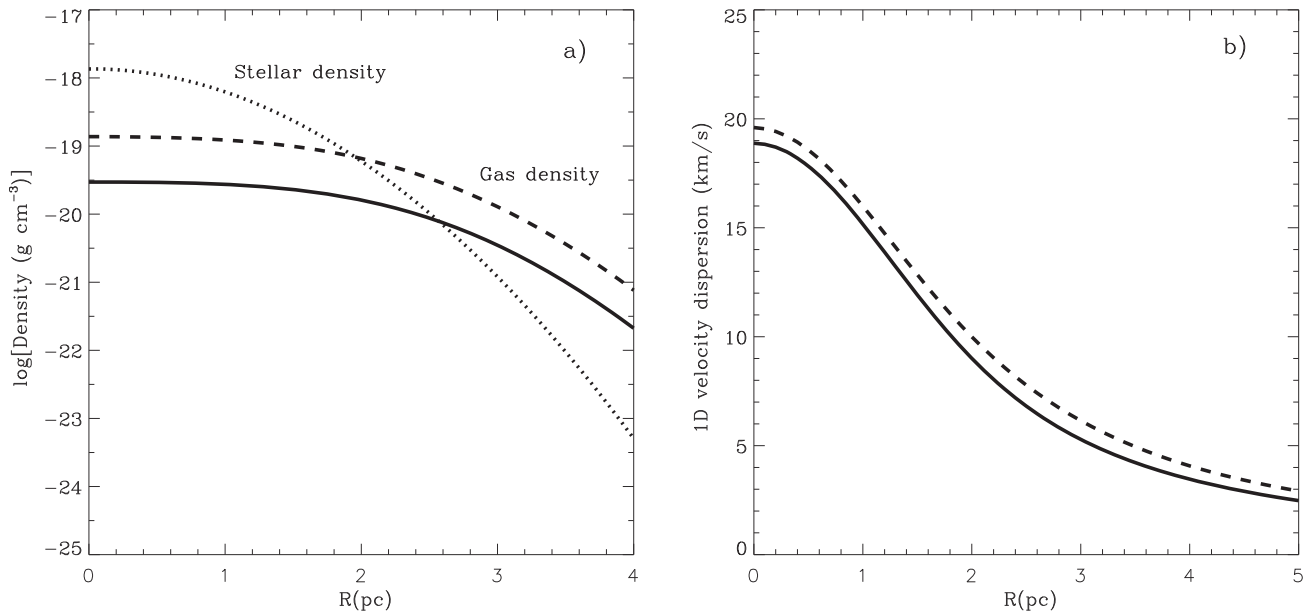


**Figure 1.** The model-predicted D1 cloud structure. The stellar mass distribution derived from the Gaussian fit to the radio and IR integrated intensity maps is shown by the dotted line in panel (a). The solid and dashed lines in this panel display the molecular gas distributions obtained for two different  $\eta_*$  factor values:  $\eta_* = 1$  (solid line) and  $\eta_* = 5$  (dashed line). The model-predicted velocity dispersions are shown on panel (b), where the solid and dashed lines correspond to the same models as in panel (a).

$L_{\text{XTT}} \approx 5 \times 10^{29} \text{ erg s}^{-1}$  is the typical luminosity of a T Tauri star (Shang et al. 2002). Massive stars emit X-rays at a level of  $\sim 10^{-7} L_{\text{bol}}$  (Crowther et al. 2022), which results in a comparable value to the T Tauri integrated value:  $L_{\text{XR,MS}} \approx 10^{-7} L_{\text{bol}} = 3.9 \times 10^{35} \text{ erg s}^{-1}$ . X-ray emission from high-mass X-ray binaries (HMXBs) may reach  $(10^{32}-10^{33})(M_{\text{SC}}/1 M_{\odot}) \text{ erg s}^{-1}$  (e.g., Mas-Hesse & Cerviño 1999; Van Bever & Vanbeveren 2000) and thus can be comparable or even exceed the turbulent heating rate. However, it takes (4–5) Myr for HMXBs to become active. Low-mass X-ray binaries (LMXBs) become active at even later times. In clusters as young as that in the center of the D1 cloud, where nonthermal radio emission from supernovae has not been detected, X-ray heating by binaries is negligible.

The estimates of the X-ray emission from hot cometary-like bubbles that form around massive stars with a strong wind are less certain as they depend on the ambient gas density and stellar parameters. Chandra observations of the UCH II regions in Sagittarius B2 (Takagi et al. 2002) and W49A (Tsujiimoto et al. 2006) revealed hard (3.0–8.0 keV) X-ray emission within the range  $10^{30} \text{ erg s}^{-1} - 10^{33} \text{ erg s}^{-1}$ , associated with some of the UCH II regions. Numerical modeling of the X-ray emission from the wind-blown bubble around the young moving star BD+60° 2522 (the Bubble Nebula) led Green et al. (2019) to find a similar soft X-ray luminosity and X-ray luminosities 1–2 orders of magnitude smaller. However, the number of massive stars with strong stellar winds is much (at least two orders of magnitude) smaller than that of T Tauri stars. Therefore it is unlikely that the integrated X-ray heating exceeds the turbulent heating rate unless the intracluster radiation field is dominated by supermassive stars (Smith et al. 2016) or the intracluster gas is exposed to external sources. Hereafter we neglect gas heating by X-rays.

The molecular gas cooling rate in this density range could be approximated by the expression (Ao et al. 2013):

$$Q_{\text{cool}} = 6 \times 10^{-29} n^{1/2} T_g^3 du/dr \text{ erg cm}^{-3} \text{ s}^{-1}, \quad (23)$$

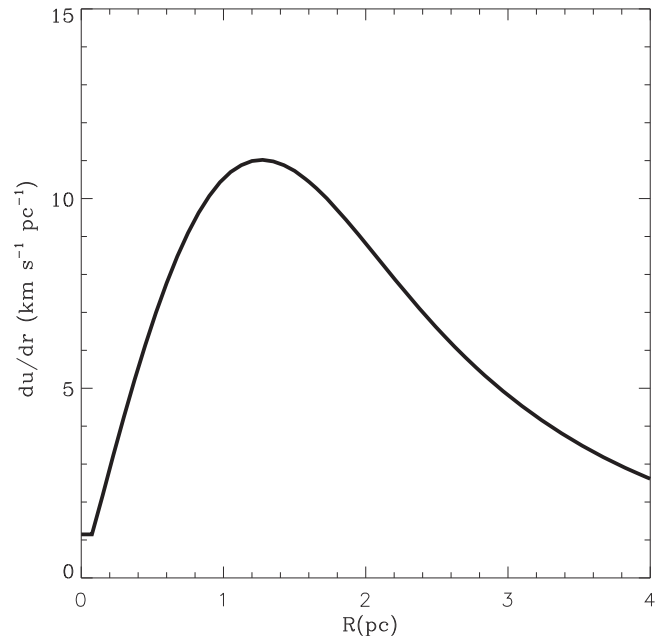


**Figure 2.** The gas velocity gradient calculated upon the assumption that  $\eta_* = 5$ .

where  $du/dr$  is the rms velocity gradient ( $du/dr = \sqrt{3d\sigma/dr}$ ) in units of  $\text{km s}^{-1} \text{ pc}^{-1}$  (see Figure 2). Note that this approximation must be taken with some care due to uncertainties in the molecular gas composition, molecule depletion onto dust grains, as well as the considered emission lines and their optical depths. If X-ray heating can be neglected and the cooling is dominated by molecular gas whose composition is determined in Table 1 of Goldsmith (2001),

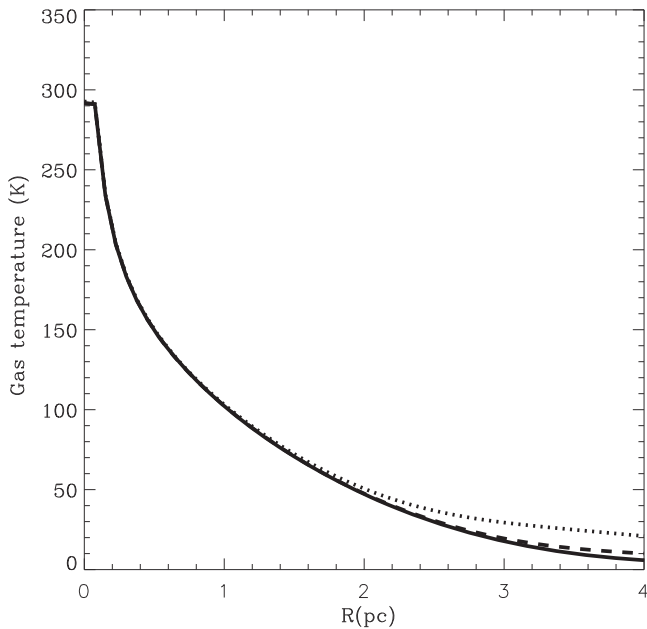


**Figure 3.** The model-predicted gas temperature distribution. The solid, dashed, and dotted lines present the model-predicted temperature distribution in the cases when the CR ionization rate is equal to that in our Galaxy, 10, and 100 times larger, respectively. The temperatures were calculated upon the assumption that  $\eta_* = 5$ .

the energy balance equation (Equation (17)) and the approximation to the gas cooling rate (Equation (23)) yield:

$$T_g = [(Q_{\text{dis}} + Q_{\text{CR}})/6 \times 10^{-29}]^{1/3} (du/dr)^{-1/3} n^{-1/6} \text{ K.} \quad (24)$$

The temperature distribution calculated upon the assumption that  $\eta_* = 5$  is shown in Figure 3. Here the solid, dashed, and dotted lines present the gas temperatures in the cases when the CR ionization rate is equal to that in our Galaxy (see Section 3.3), 10, and 100 times larger, respectively. At the Milky Way CR intensity the contribution of the CR heating is negligible. However, at starburst-like ionization rates CR heating becomes significant at the outskirts of the cluster as the turbulent heating rate per unit volume drops with radius fast, while it is likely that the CR density at the D1 cloud scale remains almost homogeneous because of large diffusion length (e.g., Aharonian et al. 2019). Large predicted molecular gas temperatures are consistent with the large CO(3–2) over CO(2–1) intensity ratio in the D1 cloud (see Turner et al. 2015). It is interesting to note that similar large temperature gradients were revealed in a sample of molecular clouds located in the central zone of the Galaxy by Rodríguez-Fernández et al. (2001) and Ao et al. (2013), who also suggested that the dissipation of supersonic turbulence could be responsible for the large molecular gas temperatures.

In the case of the D1 cloud the model predicts large star formation efficiencies:  $\approx 87\%$  in the case when parameter  $\eta_* = 1$  (which is probably not consistent with the assumption of the residual gas retention) and  $\approx 63\%$  when  $\eta_* = 5$ . The last value is in agreement with the large SFE in the D1 cloud obtained by Turner et al. (2015), the large SFE ( $\sim 47\%$ ) in the  $\rho$  Oph cloud (Wilking & Lada 1983), and agrees with the results of numerical simulations by Skinner & Ostriker (2015), who

found that the SFE may reach 50%–70% in the case of a large gas opacity to IR radiation. It is also large enough that this cluster may end up as a gravitationally bound super-star cluster (see Baumgardt & Kroupa 2007; Baumgardt et al. 2008). It is important to note that  $\eta_*$  is not a unique parameter that determines the value of the SFE. Model predictions depend also on the star cluster mass and compactness. For example, the SFE grew to 99% in simulations with  $\eta_* = 5$  and core radius  $b = 0.1$  pc. It is unlikely that at such large SFEs the individual neighboring winds and H II regions do not merge to disperse the parental cloud. We speculate here that it is the star cluster compactness that leads to a dramatic difference between the D1 cluster in NGC 5253 and the gas-free cluster R136 in the 30 Dor region, which has a similar mass and age (Portegies Zwart et al. 2010 and Mackey & Gilmore 2003 estimated the R136 core radius to fall in the range 0.1 pc–0.3 pc; see their Tables 3 and 4, respectively). On the other hand, the model-predicted SFE drops rapidly when one considers lower-mass clusters. For example, in simulations with  $\eta_* = 5$ ,  $M_{\text{SC}} = 580 M_\odot$ , and  $b = 0.14$  pc (parameters similar to the Orion Nebula cluster (ONC); Huff & Stahler 2006), we obtained  $\approx 11\%$  efficiency that agrees with the value of the SFE obtained by Huff & Stahler (2006) for ONC and Megeath et al. (2016) for different stellar groups, clusters, and clouds in the Orion complex. Certainly, the above examples should be considered only as an illustration because the stellar mass distribution in these clusters differs from a Gaussian (R136 and ONC were very well fitted by different power-law profiles). In many other cases the star cluster mass distribution is well represented by Moffat, Elson–Fall–Freeman, King, and Plummer models (see Portegies Zwart et al. 2010; Röser & Schilbach 2019; Cuevas-Otahola et al. 2020, and references therein). We leave the discussion of different stellar mass distributions to future communication.

It is instructive to note that, in spite of the large momentum input rate allowed in the simulations (up to  $5 \times L_{\text{bol}}/c$ ), the model-predicted turbulence dissipation rate remains negligibly small in comparison with the star cluster bolometric luminosity:  $2.2 \times 10^{-5} < L_{\text{dis}}/L_{\text{bol}} < 1.2 \times 10^{-4}$ . This favors radiative feedback as the major mechanism that supports turbulence in this cloud, likely through overpressurised H II regions that formed around the most massive stars as they move in the gravitational well of the cluster (e.g., Matzner 2002; Krumholz et al. 2006; Mackey et al. 2013). Indeed, a low radiative feedback efficiency is expected in dense, dusty environments (see Haid et al. 2018). This agrees with the fact that the far-infrared (FIR) luminosity of the NGC 5253 central zone ( $\approx 8 \times 10^{42}$  erg s $^{-1}$ ; Cormier et al. 2015) is comparable to and even exceeds the bolometric luminosity of the D1 cluster. In the case of a low feedback efficiency, most of the deposited energy is radiated away in the IR regime, instead of being used to unbind the residual gas. Therefore one must take care when comparing the D1 cluster with Figure 3 from Baumgardt et al. (2008), which confronts cloud binding with the accumulated radiative energy upon the assumption of a 100% radiative feedback efficiency.

Simulations with a Salpeter IMF with lower and upper cutoff masses of  $3 M_\odot$  and  $120 M_\odot$ , respectively, result in slightly larger masses of the residual gas ( $\sim 3.9 \times 10^4 M_\odot$  and  $\sim 1.5 \times 10^5 M_\odot$ ) and smaller star formation efficiencies ( $\sim 80\%$  and  $\sim 50\%$ ) in models with  $\eta_* = 1$  and  $\eta_* = 5$ , respectively.

## 5. Concluding Remarks

Here we studied the leftover gas densities, velocity dispersions, and temperatures in young stellar clusters with a given stellar mass distribution. It was postulated that star formation in the collapsing cloud is altered via the leftover gas being stirred by massive stars, which move in the gravitational well of the cluster and the residual gas. It was also assumed that if a cluster is compact and dense it can prevent the expulsion of leftover gas, and that the post-star-forming system is stable. The last condition requires the gradient of the turbulent pressure to be in balance with the gravitational pull of the cluster and the rapidly dissipated turbulent energy to be regenerated continuously. The last condition requires a sufficient number of massive stars to be formed. Therefore the steady-state condition determines both the residual gas properties and the SFE in clusters with a suppressed star cluster wind.

We confront this model with properties of a compact cluster in the nearby dwarf spheroidal galaxy NGC 5253 that is still deeply obscured by the molecular cloud D1. The model is in good agreement with several observed properties of this cluster in spite that infalling molecular filaments still supply gas to the central zone of the galaxy (Consiglio et al. 2017). It predicts the different stellar and gas density distributions with stellar mass being more concentrated toward the star cluster center. The model-predicted mass-weighted velocity dispersion is in good agreement with the observed value, while the high molecular gas temperatures are consistent with the large observed CO(3–2) to CO(2–1) intensity ratio. The large predicted SFE is sufficient for this cluster to end up as a bound super-star cluster.

The model suggests that turbulent energy dissipation may be an effective energy source for molecular gas heating in dense, compact, strongly obscured clusters, as was also suggested by Pan & Padoan (2009). It is likely that turbulent heating results in a warm molecular gas component that could be detected in FIR low-excitation emission lines of oxygen, carbon, and other species and also in millimeter/submillimeter CO rotational lines, while gas in photon dominated regions, directly heated by far-UV and X-ray photons, is manifested by high-excitation FIR lines. CO and FIR emission lines in NGC 5253 were detected by the Atacama Large Millimeter/submillimeter Array (ALMA) (see Turner et al. 2017) and Herschel (Cormier et al. 2015). The observed [O I] 63  $\mu\text{m}$  and [O I] 145  $\mu\text{m}$  line luminosities are about  $6.1 \times 10^{39} \text{ erg s}^{-1}$  at a distance of about 4 Mpc, that are larger than the model-predicted turbulent energy dissipation rate. However the Herschel observations do not separate D1 from other sources. The CO(3–2) line luminosity is smaller, about  $8.8 \times 10^{35} \text{ erg s}^{-1}$ . James Webb Space Telescope’s sensitivity and subarcsecond spatial resolution are required to reveal the contribution of the D1 cloud to the observed IR emission. It is also crucial to obtain better restrictions on the total CO luminosity and on the temperature of the warm molecular gas by observing higher  $J$  CO lines.

The fraction of stellar feedback used to regenerate the turbulent energy dissipation rate is not fixed in the present model and will be addressed in a forthcoming communication. Nevertheless, the value of the momentum input rate used in the simulations is motivated by the numerical simulations and requires that only a tiny fraction of the radiation energy be used to compensate the turbulent energy dissipation rate.

One can apply this model to clusters with an arbitrary mass distribution, but must note that it is restricted to massive and compact clusters with a suppressed mechanical feedback. It is likely, however, that our model could be also applied to lower-mass, less-compact and massive, very compact clusters with an extremely large SFE prior to their residual gas dispersal if their parental clouds are supported against gravity by turbulent pressure and contract gradually in a quasi-static regime, as was suggested by Huff & Stahler (2006) for the Orion Nebula cluster.

Certainly, the equilibrium conditions that we have used should change after the onset of supernova explosions. Further evolution of the leftover gas is beyond the scope of the present paper. We anticipate two possible scenarios: the leftover gas could be expelled out of the cluster by supernovae, which, however, is unlikely in systems with a sharp density gradient (see Jiménez et al. 2021), or the turbulent energy dissipates after the majority of massive stars explode as supernovae and the leftover gas, enriched by massive star products, collapses to form a second stellar generation.

We thank our anonymous referee for his/her constructive comments and S. Beck for careful reading of the manuscript. This study was supported by CONACYT, México research grant A1-S-28458. J.L.T. acknowledges the support of the U.S. National Science Foundation grant AST2006433. J.M. acknowledges support from a Royal Society-Science Foundation Ireland University Research Fellowship and S.M.G. acknowledges the support provided by CONACYT through Cátedra n.482.

## ORCID iDs

Sergiy Silich  <https://orcid.org/0000-0002-3814-5294>  
 Jean Turner  <https://orcid.org/0000-0003-4625-2951>  
 Jonathan Mackey  <https://orcid.org/0000-0002-5449-6131>  
 Sergio Martínez-González  <https://orcid.org/0000-0002-4371-3823>

## References

- Aharonian, F., Yang, R., & de Oña Wilhelmi, E. 2019, *NatAs*, 3, 561  
 Ao, Y., Henkel, C., Menten, K. M., et al. 2013, *A&A*, 550, A135  
 Arthur, S. J., & Hoare, M. G. 2006, *ApJS*, 165, 283  
 Basu, S., & Murali, C. 2001, *ApJ*, 551, 743  
 Baumgardt, H., & Kroupa, P. 2007, *MNRAS*, 380, 1589  
 Baumgardt, H., Kroupa, P., & Parmentier, G. 2008, *MNRAS*, 384, 1231  
 Binette, L., Flores-Fajardo, N., Raga, A. C., Drissen, L., & Morisset, C. 2009, *ApJ*, 695, 552  
 Brunt, C. M., Heyer, M. H., & Mac Low, M. M. 2009, *A&A*, 504, 883  
 Calura, F., Few, C. G., Romano, D., & D’Ercole, A. 2015, *ApJL*, 814, L14  
 Consiglio, S. M., Turner, J. L., Beck, S., et al. 2017, *ApJ*, 850, 54  
 Cormier, D., Madden, S. C., Leboutteiller, V., et al. 2015, *A&A*, 578, A53  
 Crowther, P. A., Broos, P. S., Townsley, L. K., et al. 2022, *MNRAS*, 515, 4130  
 Cuevas-Otahola, B., Mayya, Y. D., Puerari, I., & Rosa-González, D. 2020, *MNRAS*, 492, 993  
 Dalgarno, A., Yan, M., & Liu, W. 1999, *ApJS*, 125, 237  
 Elmegreen, B. G., & Scalco, J. 2004, *ARA&A*, 42, 211  
 Faucher-Giguère, C.-A., & Quataert, E. 2012, *MNRAS*, 425, 605  
 Feigelson, E. D., & Montmerle, T. 1999, *ARA&A*, 37, 363  
 Franco, J., Shore, S. N., & Tenorio-Tagle, G. 1994, *ApJ*, 436, 795  
 Goldsmith, P. F. 2001, *ApJ*, 557, 736  
 Gorjian, V., Turner, J. L., & Beck, S. C. 2001, *ApJL*, 554, L29  
 Green, S., Mackey, J., Haworth, T. J., Gvaramadze, V. V., & Duffy, P. 2019, *A&A*, 625, A4  
 Haid, S., Walch, S., Seifried, D., et al. 2018, *MNRAS*, 478, 4799  
 Henney, W. J., & Arthur, S. J. 2019, *MNRAS*, 486, 3423  
 Huff, E. M., & Stahler, S. W. 2006, *ApJ*, 644, 355

- Jiménez, S., Tenorio-Tagle, G., & Silich, S. 2021, *MNRAS*, 505, 4669
- Krumholz, M. R., Matzner, C. D., & McKee, C. F. 2006, *ApJ*, 653, 361
- Krumholz, M. R., & McKee, C. F. 2005, *ApJ*, 630, 250
- Mac Low, M.-M. 1999, *ApJ*, 524, 169
- Mac Low, M.-M., & Klessen, R. S. 2004, *RvMP*, 76, 125
- Mackey, A. D., & Gilmore, G. F. 2003, *MNRAS*, 338, 85
- Mackey, J., Gvaramadze, V. V., Mohamed, S., & Langer, N. 2015, *A&A*, 573, A10
- Mackey, J., Langer, N., & Gvaramadze, V. V. 2013, *MNRAS*, 436, 859
- Mackey, J., Walch, S., Seifried, D., et al. 2019, *MNRAS*, 486, 1094
- Maloney, P. R., Hollenbach, D. J., & Tielens, A. G. G. M. 1996, *ApJ*, 466, 561
- Marks, M., & Kroupa, P. 2012, *A&A*, 543, A8
- Mas-Hesse, J. M., & Cerviño, M. 1999, Proc. of the Symp. of the International Astronomical Union, Wolf-Rayet Phenomena in Massive Stars and Starburst Galaxies, 193 ed. K. A. van der Hucht, G. Koenigsberger, & P. R. J. Eenens (San Francisco, CA: ASP), 550
- Matzner, C. D. 2002, *ApJ*, 566, 302
- McKee, C. F. 1989, *ApJ*, 345, 782
- McKee, C. F. 1999, NATO Advanced Study Institute (ASI) Series C, The Origin of Stars and Planetary Systems, 540 ed. C. J. Lada & N. D. Kylafis (Dordrecht: Kluwer), 29
- McKee, C. F., & Ostriker, E. C. 2007, *ARA&A*, 45, 565
- Megeath, S. T., Gutermuth, R., Muzerolle, J., et al. 2016, *AJ*, 151, 5
- Meijerink, R., & Spaans, M. 2005, *A&A*, 436, 397
- Melnick, J., Moles, M., Terlevich, R., & Garcia-Pelayo, J.-M. 1987, *MNRAS*, 226, 849
- Murray, N., Quataert, E., & Thompson, T. A. 2010, *ApJ*, 709, 191
- Norman, C., & Silk, J. 1980, *ApJ*, 238, 158
- Padoan, P. 1995, *MNRAS*, 277, 377
- Padoan, P., Federrath, C., Chabrier, G., et al. 2014, in Protostars and Planets VI, ed. H. Beuther et al. (Tucson, AZ: Univ. of Arizona Press), 77
- Padoan, P., & Nordlund, Å. 2011, *ApJ*, 730, 40
- Pan, L., & Padoan, P. 2009, *ApJ*, 692, 594
- Panoglou, D., Cabrit, S., Pineau Des Forêts, G., et al. 2012, *A&A*, 538, A2
- Papadopoulos, P. P. 2010, *ApJ*, 720, 226
- Portegies Zwart, S. F., McMillan, S. L. W., & Gieles, M. 2010, *ARA&A*, 48, 431
- Quillen, A. C., Thorndike, S. L., Cunningham, A., et al. 2005, *ApJ*, 632, 941
- Rodríguez-Fernández, N. J., Martín-Pintado, J., Fuente, A., et al. 2001, *A&A*, 365, 174
- Röser, S., & Schilbach, E. 2019, *A&A*, 627, A4
- Scalo, J. M. 1987, Interstellar Processes, Astrophysics and Space Science Library, 134 ed. D. J. Hollenbach, J. Thronson, & A. Harley (Dordrecht: Reidel), 349
- Shang, H., Glassgold, A. E., Shu, F. H., & Lizano, S. 2002, *ApJ*, 564, 853
- Shu, F. H., Adams, F. C., & Lizano, S. 1987, *ARA&A*, 25, 23
- Silich, S., & Tenorio-Tagle, G. 2017, *MNRAS*, 465, 1375
- Silich, S., & Tenorio-Tagle, G. 2018, *MNRAS*, 478, 5112
- Silich, S., Tenorio-Tagle, G., Martínez-González, S., & Turner, J. 2020, *MNRAS*, 494, 97
- Skinner, M. A., & Ostriker, E. C. 2015, *ApJ*, 809, 187
- Smith, L. J., Crowther, P. A., Calzetti, D., & Sidoli, F. 2016, *ApJ*, 823, 38
- Solomon, P. M., Rivolo, A. R., Barrett, J., & Yahil, A. 1987, *ApJ*, 319, 730
- Stone, J. M., Ostriker, E. C., & Gammie, C. F. 1998, *ApJL*, 508, L99
- Swift, J. J., & Welch, W. J. 2008, *ApJS*, 174, 202
- Takagi, S.-i., Murakami, H., & Koyama, K. 2002, *ApJ*, 573, 275
- Tenorio-Tagle, G., Muñoz-Tunon, C., & Cox, D. P. 1993, *ApJ*, 418, 767
- Terlevich, R., & Melnick, J. 1981, *MNRAS*, 195, 839
- Tsujimoto, M., Hosokawa, T., Feigelson, E. D., Getman, K. V., & Broos, P. S. 2006, *ApJ*, 653, 409
- Turner, J. L., Beck, S. C., Benford, D. J., et al. 2015, *Natur*, 519, 331
- Turner, J. L., Beck, S. C., & Ho, P. T. P. 2000, *ApJL*, 532, L109
- Turner, J. L., Consiglio, S. M., Beck, S. C., et al. 2017, *ApJ*, 846, 73
- Van Bever, J., & Vanbeveren, D. 2000, *A&A*, 358, 462
- Vazquez-Semadeni, E., Ostriker, E. C., Passot, T., Gammie, C. F., & Stone, J. M. 2000, in Protostars and Planets IV, ed. V. Mannings, A. P. Boss, & S. S. Russell (Tucson, AZ: Univ. of Arizona Press), 3
- Wareing, C. J., Zijlstra, A. A., & O'Brien, T. J. 2007, *ApJL*, 660, L129
- Whitworth, A. P. 2016, *MNRAS*, 458, 1815
- Wilking, B. A., & Lada, C. J. 1983, *ApJ*, 274, 698
- Williams, J. P., & McKee, C. F. 1997, *ApJ*, 476, 166
- Wirth, H., Kroupa, P., Haas, J., et al. 2022, *MNRAS*, 516, 3342